Front. Environ. Sci. Eng. 2021, 15(6): 130
https://doi.org/10.1007/s11783-021-1418-2

RESEARCH ARTICLE

Enhancing the adsorption function of biochar by mechanochemical graphitization for organic pollutant removal

Peidong Su [1#], Xiangyu Gao [2#], Junke Zhang[1], Ridha Djellabi[1], Bo Yang (✉)[1], Qi Wu[3], Zhen Wen[1]

1 College of Chemistry and Environmental Engineering, Shenzhen University, Shenzhen 518060, China
2 State Key Laboratory of Urban Water Resources and Environment, School of Environment, Harbin Institute of Technology, Harbin 150090, China
3 Senior 3, Houde Academy, Shenzhen 518000, China

HIGHLIGHTS

- Mechanochemical treatment reduced the calcination temperature for biochar synthesis.
- Biochar is converted to graphite after mechanochemical treatment.
- Biochar was reduced to nanoscale after mechanochemical treatment.

GRAPHIC ABSTRACT

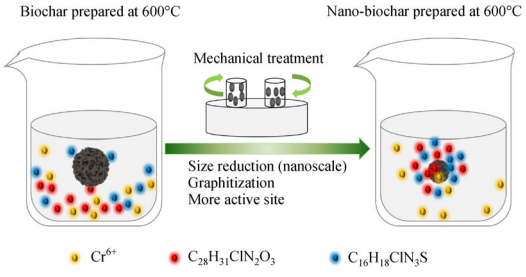

ARTICLE INFO

Article history:
Received 16 November 2020
Revised 6 February 2021
Accepted 16 February 2021
Available online 25 March 2021

Keywords:
Biochar
Mechanochemical treatment
Graphitization
Calcination temperature
Organic pollutant

ABSTRACT

Biochar (BC) has been extensively studied as adsorbent for the treatment of water pollution. Despite the distinct advantages, the high calcination temperature and low adsorption capacity of pristine BC limit its practical applications. Most of the former studies focused on the structure and/or surface modification to improve the adsorption capacity of BC. However, the harsh experiment conditions involved in the biochar modification limited the application in industrial level. Herein, we introduced mechanical treatment into BC preparation to reduce the calcination temperature and improve the adsorption capacity simultaneously. The results indicated that the calcination temperature was reduced and the adsorption capacity of the treated BC was improved after mechanochemical treatment. Characterization of the samples disclosed that BCs were graphitized with the particle size reduced to nanoscale after treatment. Adsorption tests indicated that the mechanochemically treated BCs showed much better removal performance of organic contaminants than that of pristine BCs. For instance, among four pristine BCs (BC600, BC700, BC800, and BC900), only BC900 has strong adsorption capacity for MB, while BC600 has low adsorption capacity (1.2 mg/g). By comparison, the adsorption capacity of MB increased greatly to 173.96 mg/g by BC600-500/1 (treated at 500 r/min for 1 hour). To optimize the mechanochemical treatment, the effects of rotation speed and agitation duration were also investigated.

1 Introduction

The conversion of carbon-rich biomass into value-added materials is a promising strategy for reusing natural resources (Liu et al., 2015; Zhang et al., 2020a). Many carbonaceous materials include but not limited to activated carbon (AC) (Ao et al., 2018; Liu et al., 2019; Ajmani, et al., 2020), biochar (BC) (Rajapaksha et al., 2016; Sizmur et al., 2017; Bakshi et al., 2018), carbon nanotube (CNT) (Yao et al., 2017; Zhang et al., 2018; Zhang et al., 2019), and graphene (Choi et al., 2018; Lu et al., 2020) can be prepared using different kinds of biomass feedstock. Among them, BC is the most widely studied product derived from biomass due to its potential applications in energy storage, contaminants removal, and gas separation and storage (Liu et al., 2015). Alternatively, biomass calcination is an important route for BC preparation.

✉ Corresponding author
E-mail: boyang@szu.edu.cn

[#]These two authors contributed equally to this article

Biomasses such as rice husk, wheat straw, hickory chips, etc. are heated in the absence of oxygen to prepare BC (Sun et al., 2014; Peters et al., 2015; Zhang et al., 2015; Li et al., 2017a). The physicochemical properties (i.e., surface area, pore structure and size distribution, and surface functional groups) of BC strongly depend on the compositions of feedstock, temperature, and calcination process (Yu et al., 2017; Kim et al., 2020). However, pristine BCs that are prepared at low-temperature usually have low adsorption capacity because the pore structure and surface functional groups are not well developed.

The basic strategy for the improvement of the adsorption capacity of BC is the optimization of the calcination process (Li et al., 2017a; He et al., 2018). The surface structure, ash content, surface functional groups and thermal stability, etc. are significantly affected by the calcination temperature and heating rate. In common cases, the higher the temperature, the more developed the pore structure of BC, and the adsorption ability for pollutants would increase accordingly. However, there is an inevitable problem that energy consumption will increase with the increase of calcination temperature. Xu et al. (Xu et al., 2019) investigated the properties of hickory chips (HC)- and bagasse (BG)-derived BCs at calcination temperature ranged from 450°C–600°C. The results showed that the specific surface area of synthesized BC at 450°C was very small, 7.36 and 88.5 m^2/g for HC450 and BG450, respectively. When the calcination temperature increased to 600°C, the specific surface area of HC600 and BG600 increased to 370 and 196 m^2/g, respectively. As a result, the adsorption capacity of HC and BG was improved, accordingly. Therefore, in order to harvest BCs with high sorption capacity, a high temperature is usually needed.

Another strategy for the reinforcement of the adsorption capacity of BC is surface modification. Different chemical methods such as acid/alkaline activation, nanoparticle loading, and magnetization have been employed to modify BC for different purposes (Cheng et al., 2017; Huang et al., 2019; Kim et al., 2019; Zhang et al., 2020b). For instance, different kinds of pine sawdust-derived BCs were synthesized by Huang et al. (2019) and modified by 3-mercaptopropyltrimethoxysilane (3-MPTS). The thiol-modified BCs showed exciting removal performance for aqueous Hg^{2+} and CH_3Hg^+. In another study by Li et al. (2017b), magnetic BCs were prepared by $Fe(NO_3)_3$ and rice straw at 400°C, 600°C, and 800°C, respectively. They found that the removal efficiency of aromatic contaminants (anisole and phenol) by the magnetic BCs followed the order: MB 600 > MB 800 > MB 400. Moreover, publications have also reported the BC-supported photocatalysts for organic pollutants degradation in water purification (Ye et al., 2019; Talukdar et al., 2020; Zhang et al., 2020c).

Nevertheless, surface modification usually reduces the adsorption performance of raw BC since the limited active sites on the BC would be occupied by the loaded substances (Tian et al., 2017; Lu et al., 2019; Djellabi et al., 2020; Kumar et al., 2020). Besides, the harsh experiment conditions involved in chemical modification limit the wide application at industrial level. Comparatively, mechanochemistry, which is well known as ball milling, is considered as a cost-efficient, environmentally sound, facile, and solvent-free technique for BC modification (Lyu et al., 2018; Xu et al., 2019). There is no need to introduce chemicals into BC during ball milling. Under the treatment of high mechanical energy, the surface charge and chemical bonds will be changed and the particle size of the processed BC will be reduced to nanoscale along with the milling medium (Kumar et al., 2020). In addition, ball milling is usually associated with crystal deformation and temperature increase, which can improve the activity of BC and reduce the biomass calcination temperature for BC preparation (Julien et al., 2016; Do and Friscić, 2017; Teng et al., 2017).

Therefore, the specific objective of this study was to improve the adsorption capacity of BC and reduce the calcination temperature using mechanochemical treatment. Different kinds of coconut bran-derived BCs were prepared at different calcination temperatures (600°C, 700°C, 800°C, and 900°C) under N_2 protection, followed by ball milling process under various conditions. The adsorption performance of the BCs was examined by removing organic pollutants (methylene blue (MB), rhodamine B (RHB)), and inorganic pollutant (Cr^{6+}) in aqueous solution. The effects of calcination temperature, initial concentration of contaminant, pH, rotation speed, and agitation duration were investigated to optimize the conditions for BC preparation.

2 Materials and methods

2.1 Materials

Coconut bran collected from farmland was used as feedstock for BC preparation. Potassium dichromate ($K_2Cr_2O_7$, 99.8%), sodium hydroxide (NaOH, 96%), rhodamine B ($C_{28}H_{31}ClN_2O_3$, 99.75%), hydrochloric acid (HCl, 36%–38%), and methylene blue trihydrate ($C_{16}H_{18}ClN_3S\cdot 3H_2O$, 99.5%) were bought from Sinopharm Chemical Reagent Co., Ltd. (China). All the chemicals were used as received without purification. Ultra-purified water (ρ = 18.2 MΩ·cm) was prepared using a purification system (Millipore, Billerica, MA, USA) and used throughout the experiment.

2.2 BC preparation

The pristine BCs were prepared by heating the Coconut bran to 600°C, 700°C, 800°C, and 900°C under N_2 protection for 6 h at a heating rate of 3°/min, respectively. The obtained BCs were ground evenly until no obvious flocks, and followed by washing with ultra-purified water

three times. After dried at 105°C for 12 h, the samples were collected and named BC600, BC700, BC800, and BC900, respectively.

Ball milling of the above prepared BCs was conducted in a planetary ball-milling machine (Fristch Pulverisette7, Germany). The agate jars and balls are all made of zirconia (ZrO_2). In brief, 200 mg raw BC was mixed with 7 balls (7 × 10 g) in the jar and milled at designed speed and duration with rotation direction altered every 10 min. The harvested BCs were named in the form of calcination temperature-speed/duration. For example, BC600-500/2 means the BC was synthesized at 600°C and milled at 500 r/min for 2 h. To optimize the activation process, the milling speed was set to be 100, 200, 300, 400, and 500 r/min, respectively, and the milling duration was set to be 0.5, 1.0, 1.5, and 2.0 h.

2.3 Material characterization

The surface functional groups of the selected BCs were determined using Fourier transform infrared (FT-IR) spectrometer (Nicolet 8700, Thermal Fisher Scientific, USA) with an ESCALAB250Xi spectrometer. To determine the specific surface area and pore size of the BCs, N_2 adsorption and desorption isotherms were analyzed using AUTOSORB-1 surface area and pore size analyzer (Quantachrome, USA). The crystallinity of the BCs before and after ball milling was evaluated by X-ray diffraction (XRD) using a X` Pert Pro (Bruker, Germany) equipped with a Cu Kα radiation source at 40 mA and 40 kV. The surface morphologies of the BCs were analyzed by Scanning Electron Microscopy- Energy Dispersive Spectrometer (SEM-EDS) (Hitachi SU8020, Japan). To determine the chemical bonds involved in the samples, X-ray photoelectron spectroscopy (XPS) was carried out.

2.4 Adsorption test

In this study, the adsorption performance of MB, RHB and Cr^{6+} ions by raw BCs and ball milled-BCs were conducted in aqueous solution. Typically, 0.05 g BC was added into 100 mL of MB, RHB or Cr^{6+} solution at designed concentrations. The mixture was then stirred at 300 r/min for 180 min at room temperature. About 1.5 mL of the sample was taken out at designed intervals using a syringe and filtered through 0.45 μm filter for UV-vis analysis (UV-Vis 2600, Shimadzu, Japan). For MB and RHB, organic phase syringe filter was used while water phase syringe filter for Cr^{6+} solution. The effect of initial pH on the adsorption ability of BCs was evaluated with the initial pH of 2.0, 4.0, 8.0, 10.0, and 12.0, respectively. The pH of the solutions was adjusted using 1 M HCl or 2 M NaOH. The adsorption capacity of MB, RHB, and Cr^{6+} by each BC was calculated using Eq. (1):

$$q = (C_0 - C_e)V/m, \quad (1)$$

where, q is the adsorption capacity of pollutant (mg/g), V is the solution volume (100 mL), m is the dosage of BC (0.05 g), and C_0 and C_e (mg/L) is the initial and equilibrium concentration of contaminant, respectively.

2.5 Adsorption isotherm and kinetic analyses

To investigate the adsorption isotherm, 0.05 g BC was mixed with 100 mL MB, RHB, and Cr^{6+} solutions with different initial concentrations at room temperature. Langmuir (Langmuir, 1918) and Freundlich (Freundlich, 1906) adsorption isotherms were employed to simulate the adsorption process of selected pollutants. The corresponding equations of the two isotherms are as follows (Eq. (2)):

$$\text{Langmuir isotherm}: \frac{C_e}{q_e} = \frac{1}{K_L Q_{max}} + \frac{C_e}{Q_{max}}, \quad (2)$$

$$\text{Freundlich isotherm (Eq.(3))}:$$

$$\ln q_e = \ln K_F + \frac{1}{n}\ln C_e, \quad (3)$$

In the above equations, Q_{max} (mg/g) represents the maximum adsorbed quantity of contaminants, K_L (L/mg), K_F (L/g) are Langmuir and Freundlich isotherm constants, respectively. $1/n$ indicates the heterogeneity of the adsorbent's surface. Usually, the smaller $1/n$ is, the more heterogeneous the surface will be.

The adsorption kinetics analysis of MB, RHB, and Cr^{6+} by raw BC and ball milled-BCs was investigated through pseudo-first-order model (Lagergreen, 1898) (Eq. (4)) and pseudo-second-order model (Ho and McKay, 1998) (Eq. (5)), respectively:

$$\ln(q_e - q_t) = \ln q_e - k_1 t, \quad (4)$$

$$\frac{t}{q_t} = \frac{1}{k_2 q_e^2} + \frac{t}{q_e}, \quad (5)$$

where q_e (mg/g) and q_t (mg/g) are the quantity of contaminants removed at equilibrium and time t, respectively. k_1 (min^{-1}) and k_2 (g/mg/min) represent the reaction constant of pseudo-first order and pseudo-second order model, respectively.

3 Results and discussion

3.1 Characterization of raw BCs and ball milled-BCs

To identify the inner structure of prepared BCs, XRD tests were performed. As shown in Fig. 1(a), two specific peaks were identified. The peak located around 20.6° was attributed to amorphous carbon ((PDF#26–1076 (006) and/or PDF#26–1080 (004)) (Jonidi Jafari et al., 2017). The peaks around 26.6° were identified as graphite (PDF#99–0057). Compared the raw BCs with ball milled

BCs, the peak intensities of graphite in ball milled BCs were enhanced which revealed that ball milling could promote the graphitization of BCs.

To examine the variation of functional groups in BC after mechanochemical treatment, FTIR analysis was performed on BC600, BC900, BC600-500/2, and BC900-500/2. As shown in Fig. 1(b), the small peak at about 1368 cm^{-1} should be in-plane bending of-OH, while peaks at about 3600 cm^{-1} correspond to the-OH stretching. It is obvious that the -OH stretching was enhanced significantly after mechanochemical treatment. The band at 2917 cm^{-1} was identified as aliphatic C-H wags, and band at 1647 cm^{-1} represented C = C stretching. C = O band stretching usually appeared at about 1560 cm^{-1}, and in this study, the adown band at 1557 cm^{-1} should be -COOH (Sun et al., 2014; Xiao et al., 2019). The BC prepared at 600°C have much stronger-COOH band than that of BCs prepared at 900°C, indicating that -COOH would be destroyed with temperature increasing. By comparing the -COOH band for BC600 and BC600-500/2, it can be concluded that mechanochemical treatment can improve the intensity of -COOH.

N_2 adsorption-desorption analyses were further performed on BC600, BC900, BC600-500/2, and BC900-500/2 to investigate the variation of pore structure. As shown in Fig. 2(a), all the samples show type IV adsorption-desorption isotherm with an H1 hysteresis loop, indicating mesoporous structure of them (Tran et al., 2017; Li et al., 2018; Su et al., 2020b; Tang et al., 2020a). This is further proved by the pore size distribution of BC600, BC900, BC600-500/2, and BC900-500/2 as presented in Fig. 2(b). The average pore sizes of BC600, BC900, BC600-500/2, and BC900-500/2 were 31.61, 36.78, 39.54, and 17.23 nm, respectively (Table 1).

In the meanwhile, the specific surface area of the four types of BCs followed the order of BC900-500/2 (245.598 m^2/g)>BC600-500/2 (162.847 m^2/g)>BC900 (139.290 m^2/g)>BC600 (45.536 m^2/g). Obviously, ball milling can improve the specific surface area of the BCs significantly.

As shown in Fig. S1(a), the full survey XPS spectra of BC600, BC900, BC600-500/2, and BC900-500/2 indicated that C1s (Fig. S1(b)) and N1s (Fig. S1(c)) were identified. However, from Fig. S1(c) it can be found that N was only detected in sample BC900-500/2. Through high-resolution XPS spectra (Fig. 3), C = C (284.8 eV), C-O (286.5 eV) and C = O (288.4 eV) were detected in both BC600 and BC900. By comparison, C-O (286.5 eV) and C = O (288.4 eV) disappeared after ball milling, while C-C (285.9 eV) was detected in BC600-500/2 and BC900-500/2. This phenomenon further confirmed that graphitization of BCs during ball milling process.

According to the former studies, one of the main advantages of ball milling is size adjustment, and the particle size of the ball milled sample would be reduced to nanoscale (Tsuzuki and McCormick, 2004; Yang et al., 2004; Biswal et al., 2013). As shown in Fig. 4(a), there are big blocks and lamellar structures with a size of tens of micros in BC600, BC700, and BC800. These big blocks and lamellar structures should be unburnt substances of the coconut bran. The morphology of BC900 in Fig. 4(a)

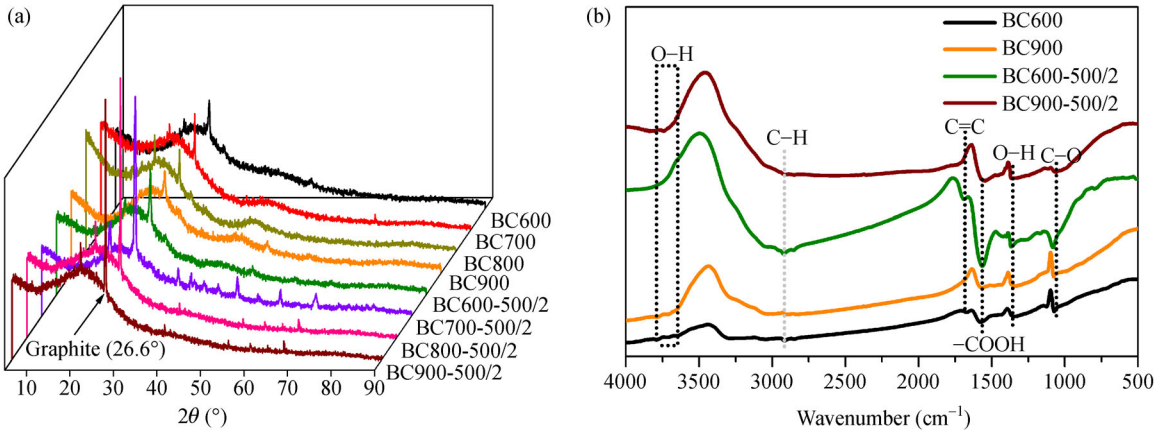

Fig. 1 (a) XRD patterns of BCs, and (b) FTIR plots of BC600, BC900, BC600-500/2, and BC900-500/2.

Table 1 Specific surface area (SSA) and pore structure of BC600, BC900, BC600-500/2, and BC900-500/2

Sample	SSA (m^2/g)	Pore volume (cm^3/g)	Pore size (nm)
BC600	44.536	0.0704	31.61
BC600-500/2	162.847	0.2994	36.78
BC900	139.290	0.2753	39.54
BC900-500/2	245.598	0.2116	17.23

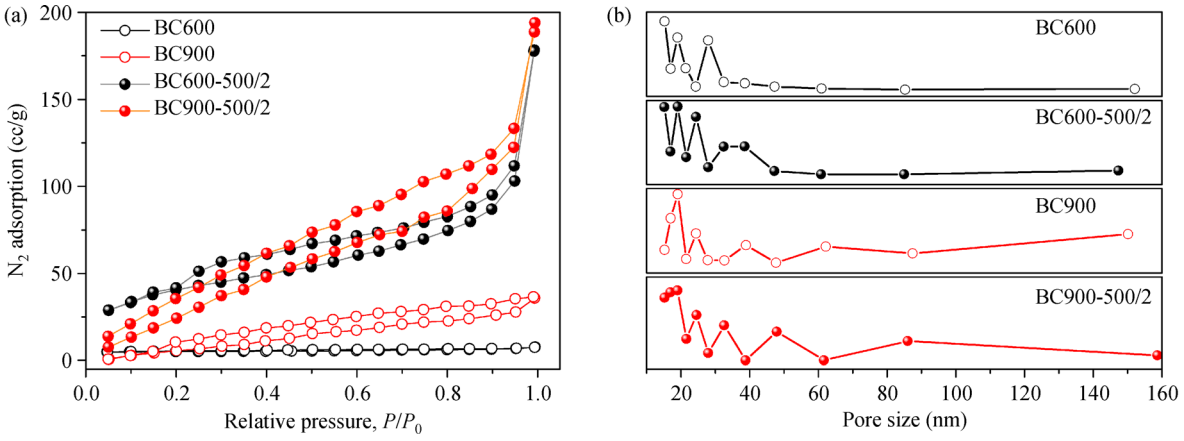

Fig. 2 N_2 adsorption and desorption isotherms (a) and pore size distribution of BC600, BC900, BC600-500/2, and BC900-500/2 (b).

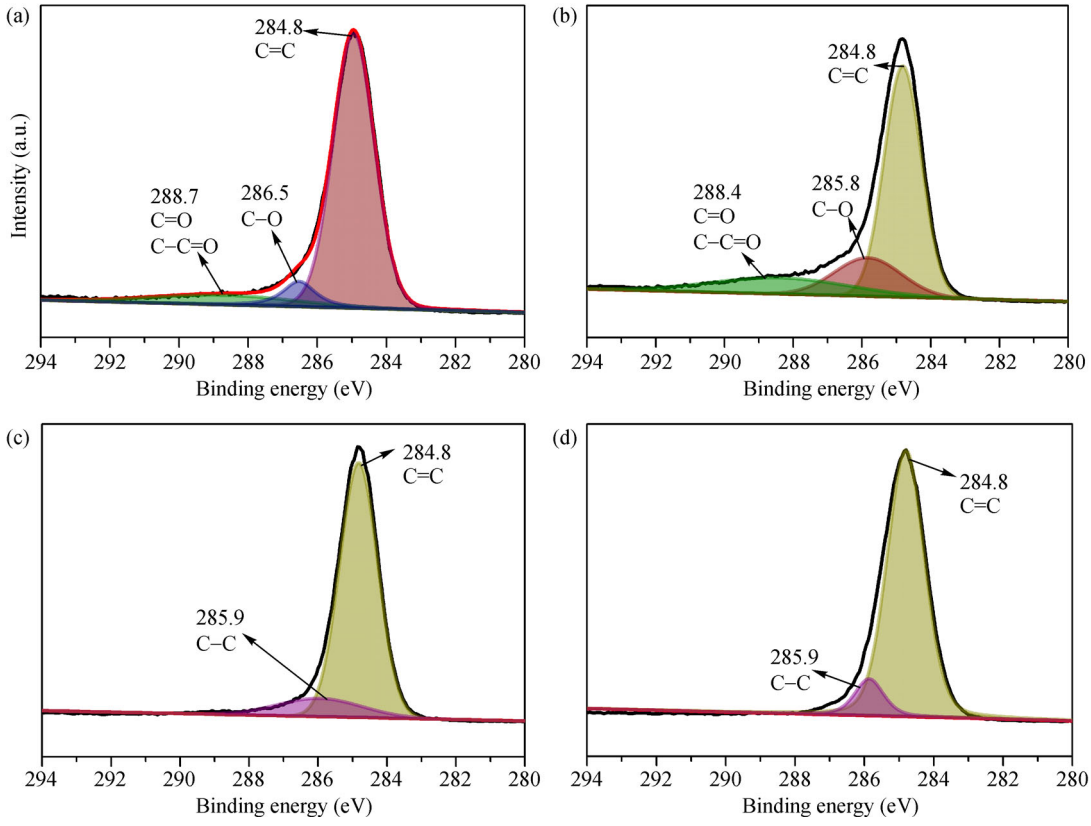

Fig. 3 High resolution of C1s of BC600 (a), BC900 (b), BC600-500/2 (c), and BC900-500/2 (d).

showed that there were less lamellar structures left as compared to the other three raw BCs. This is reasonable because the higher the temperature, the more complete the combustion and structural damage. After ball milling, as shown in Fig. 4(b), lamellar structures disappeared, and the particle size of the milled BCs was reduced to nanometer size. In this case, there were more active sites available on the surface of ball milled BCs. The element distribution analysis in Fig. 4(c) indicated that C, N, S, and O were four dominant elements in the coconut bran-derived BCs.

3.2 MB removal by raw BCs and ball milled-BCs

3.2.1 Effect of ball milling on MB removal

In this study, the adsorption performance of synthesized BCs and ball milled- BCs was firstly evaluated through the removal of MB at 10 mg/L. As shown in Fig. 5(a), the adsorption of MB was negligible by raw BC600, BC700, and BC800. The equilibrant removal efficiency of MB was only 11.2%, 24.0%, and 28.7% for BC600, BC700, and

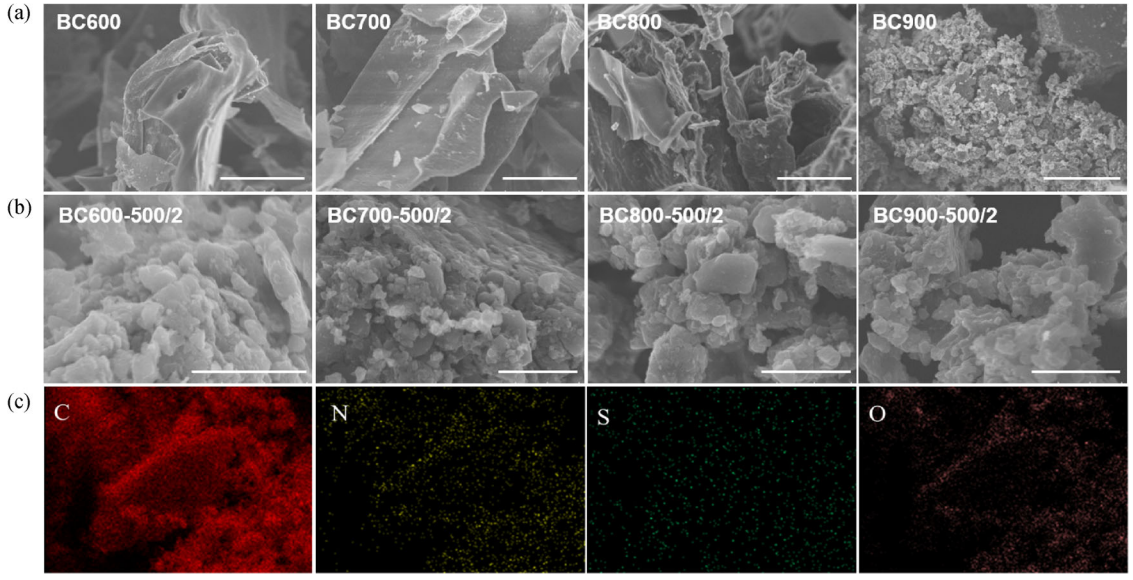

Fig. 4 (a) SEM images of BC600, BC700, BC800, BC900 (Scale bar, 10 μm), (b) SEM images of BC600-500/2, BC700-500/2, BC800-500/2, BC900-500/2 (Scale bar, 1 μm), and (c) C, N, S, and O distribution on BC900-500/2.

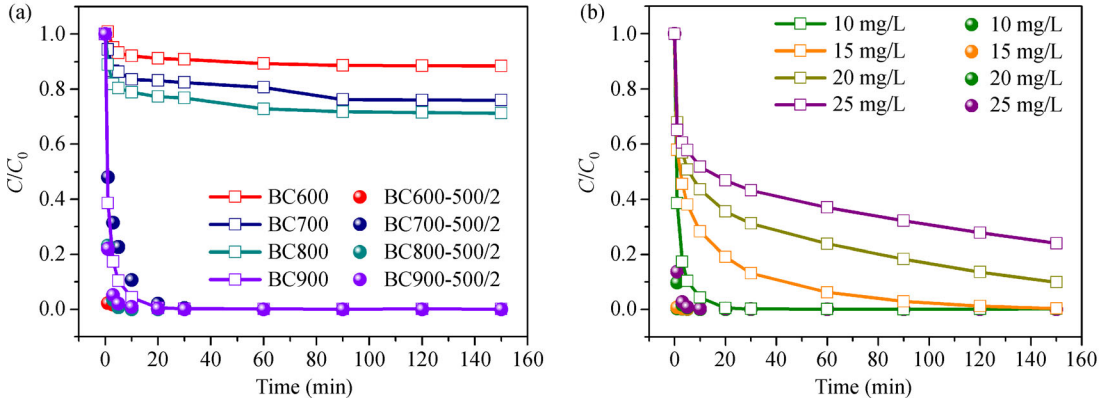

Fig. 5 The removal efficiency of MB by different BCs (a) (adsorbent dosage = 0.05 g, MB concentration = 10.0 mg/L, solution volume = 100.0 mL), and the effect of initial concentration on the adsorption of MB by BC900 and BC900-500/2 (b) (adsorbent dosage = 0.05 g, solution volume = 100.0 mL, lines for BC900 and dots for BC900-500/2).

BC800, respectively. When it comes to BC900, the removal efficiency of MB was increased greatly to about 100% after 30 min continuous adsorption, indicating that the adsorption capacity of raw coconut bran-derived BCs was strongly affected by calcination temperature. By comparison, the ball milled-BCs showed much better performance on MB removal. The removal efficiency of MB by BC600-500/2 increased to 97.8% at 1 min and 100% at about 10 min, which is much faster than that of raw BC900 (61.5% at 1 min, and 95.7% at 10 min). Similarly, the other three ball milled BCs, BC700-500/2, BC800-500/2, and BC900-500/2 showed much better performance on MB removal than their originated BCs, and all of them can remove MB completely with 30 min.

In order to further investigate the effect of ball milling on the improvement of MB removal, the adsorption of MB at different concentrations by BC900 and BC900-500/2 were tested. As shown in Fig. 5(b), the removal efficiency of 10, 15, 20, and 25 mg/L MB by BC900 at 150 min were 99.8%, 99.6%, 90.1%, and 76.0%, respectively. For BC900-500/2, different gradients of MB were completely absorbed within 10 min. Therefore, ball milling can not only improve the adsorption capacity of coconut bran-derived BC but also boost the adsorption process.

3.2.2 Effect of rotation speed on MB removal

Rotation speed is one of the main factors that affect the activation of BC since kinetic energy generated during ball milling process strongly depends on the motion of

agitating balls. Besides, the rupture of chemical bond and macromolecules is mainly determined by rotation speed. In order to examine the effect of rotation speed on MB removal, the ball milling was conducted at 100, 200, 300, 400, and 500 r/min for a period of 2 h. The harvested ball milled BCs were then employed to the removal of 100 mL 10 mg/L of MB. The removal efficiency of MB by ball milled BCs obtained at 500 r/min is presented in Fig. 5, and the results of MB removal by BCs obtained at 100, 200, 300, and 400 r/min are given in Fig. 6. As shown in Fig. 6 (a), the adsorption of MB by BCs was hardly improved when the rotation speed was 100 r/min. In fact, we noticed that the motion of balls was mild at 100 r/min during experiment. The motion of balls at 100 r/min was rather mild, and little kinetic energy was generated. As a result, there was little possibility to active BC. However, when the rotation speed increased to 200 r/min, the removal efficiency of MB increased significantly. As shown in Figs. 6(b)–6(d), MB can be completely removed within 30 min by ball milled BC600, BC700, BC800, and BC900. It is clear that the higher rotation speed would lead to better removal efficiency for MB. However, the higher rotation speed would result in higher energy consumption. Thus, 200 r/min was selected as the optimal rotation speed.

3.2.3 Effect of ball milling duration on MB removal

Ball milling duration is another important factor that affects the adsorption capacity of ball milled BC. It is generally believed that within a certain time range, the adsorption capacity of BC increases with the increase of the ball milling time, while excessive ball milling has little effect on the improvement of adsorption capacity of BC. Besides, too long ball milling time may cause the destruction of BC structure as well as much energy consumption. Therefore, it is necessary to determine the optimal ball milling time. For the adsorption of MB, we have previously determined that the optimal ball milling speed is 200 r/min. Therefore, in the experiment to determine the optimal ball milling time, we chose to run at 200 r/min. As seen in Fig. S2(a), after ball milling at 200 r/min for 0.5 h, 0.05 g of BC700-200/0.5, BC800-200/0.5, and BC900-200/0.5 can completely remove 100 mL 10 mg/L of MB within 10 min. In particular, the adsorption capacity of BC700-200/0.5 and BC800-200/0.5 was much higher than that of raw BC700 and BC800, respectively. In contrast, the maximum removal efficiency of MB by BC600-200/0.5 was only about 82.2% after 150 min of continuous reaction. When the ball milling time increased

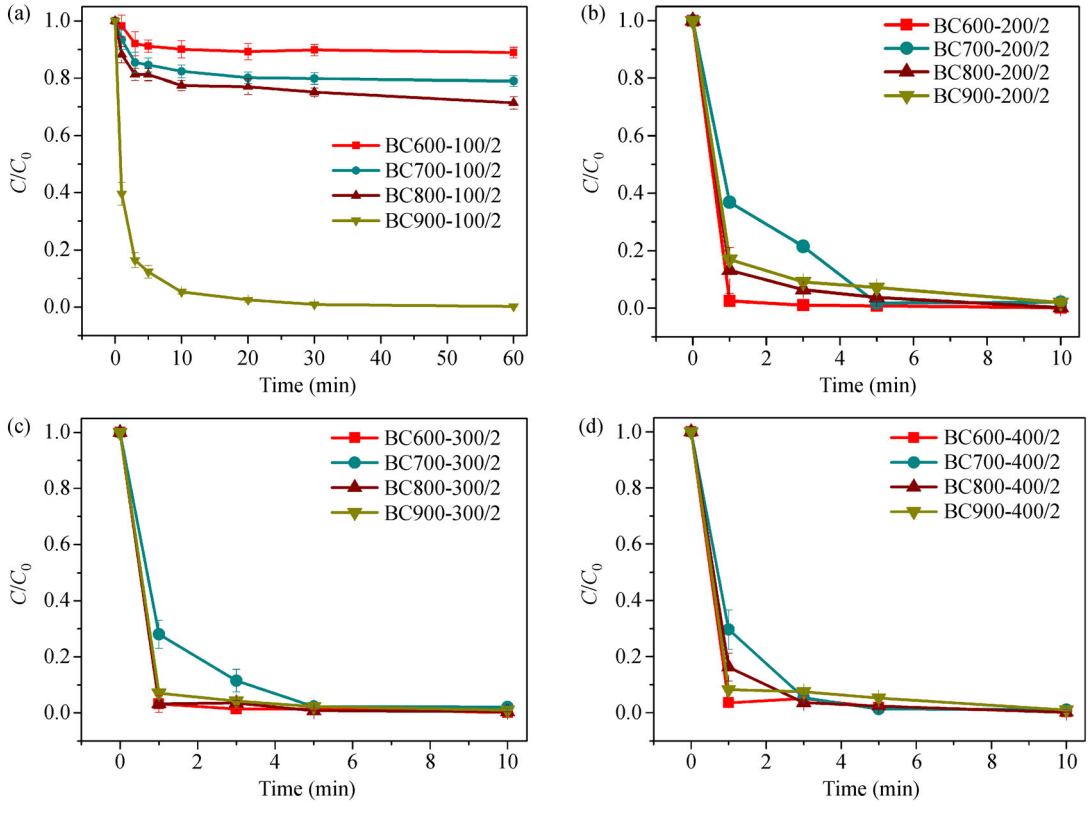

Fig. 6 The effect of rotation speed on the removal efficiency of MB by BCs Agitation speed = 100 r/min (a), 200 r/min (b), 300 r/min (c), and 400 r/min (d) (adsorbent dosage = 0.05 g, MB concentration = 10.0 mg/L, solution volume = 100.0 mL).

to 1 h, BC600-200/1 can remove all MB in about 60 min (Fig. S2(b)). After that, with the increase in ball milling time, the time for the complete removal of MB reduced gradually. But as mentioned earlier, reducing ball milling time means reducing costs, the optimal ball billing time was chosen to be 1 h. compared to other adsorbents for the adsorption of MB, BC900-200/1 outranked other BCs due to its superior adsorption performance and energy saving.

3.3 RHB removal by raw BCs and ball milled-BCs

Compared with easily adsorbed MB, RHB with low adsorption was selected as another pollutant to further examine the effect of ball milling on the improvement of adsorption of BC. Similarly, 0.05 g of different adsorbents were used to adsorb 100 mL 10 mg/L of RHB. As shown in Fig. 7(a), the maximum removal efficiency of RHB was obtained by BC900, which is about 64.3%. The removal efficiency of RHB by BC600, BC700, and BC800 were only 20.0%, 22.2%, and 23.6%, respectively. After milling at 500 r/min for 2 h, the removal efficiency of RHB by BC600-500/2 increased to 96.0%. And BC700-500/2, BC800-500/2, and BC900-500/2 can completely remove RHB in about 30 min. In addition, the investigation of the effect of initial concentration on the removal of RHB indicated that RHB can be removed in depth by BC900-500/2 in about 30 min when the RHB concentration ranged from 5 to 20 mg/L (Fig. 7(b)). From Fig. S3, it can be found that the RHB removal efficiency by BC900-200/2 was about 98.9%. In contrast, RHB removal efficiency by BC600-200/2, BC700-200/2, and BC800-200/2 were 63.9%, 73.74%, and 87.7%, respectively.

The milled four BCs were able to remove all RHB in about 30 min after milling at 200 r/min for 2 h (Fig. S3). The effect of ball milling time on RHB removal is presented in Fig. 8. As can be seen in Fig. 8, the removal efficiency of RHB was significantly improved by all milled BCs as compared with raw BCs. For instance, the removal efficiency of MB was 37.3%, 46.4%, 67.1%, and 89.3% by BC600-200/0.5, BC700-200/0.5, BC800-200/0.5, and BC900-200/0.5, respectively. Overall, the RHB removal efficiency increased with the increase of ball milling time. However, only BC900-200/1.5 and BC900-200/2 could remove RHB completely after about 90 min. Thus, to remove 100 mL 10 mg/L of RHB, the ball milling time should be no less than 1.5 h. In this study, we chose BC900-200/1.5 as the ideal adsorbent for RHB removal.

3.4 Cr^{6+} removal by raw BCs and ball milled-BCs

In addition to the above-mentioned two organic pollutants, the adsorption of metal ions by coconut bran-derived BC before and after ball milling was also studied. As a hazardous metal in water, Cr(VI) was selected as a probe to evaluate the adsorption ability of BC. The results are given in Fig. S4. Obviously, BCs before and after ball milling showed poor adsorption for Cr(VI). The removal efficiency of Cr(VI) by raw BC600, BC700, BC800, and BC900 were only 1.7%, 2.0%, 2.9%, and 4.7%, respectively as shown in Fig. S4(a). To investigate the removal efficiency of Cr(VI) by ball milled BCs, BC900 for milling at 500 r/min for different time was selected. As shown in Fig. S4(b), the maximum removal efficiency of Cr(VI) was obtained by BC900-500/2 (7.7%). While removal efficiency of Cr(VI) was only 4.8%, 6.4%, and 7.4% by BC900-500/0.5, BC900-500/1, and BC900-500/1.5, respectively. It is worth noting that BC900-200/2, which showed great adsorption of MB and RHB, did not show adsorption for Cr(VI). It is believed that BC prepared with coconut bran obtained a negligible adsorption effect on the removal of metal ions.

3.5 The effect of solution pH on contaminant removal by ball milled-BCs

Considering that pH can significantly affect the removal

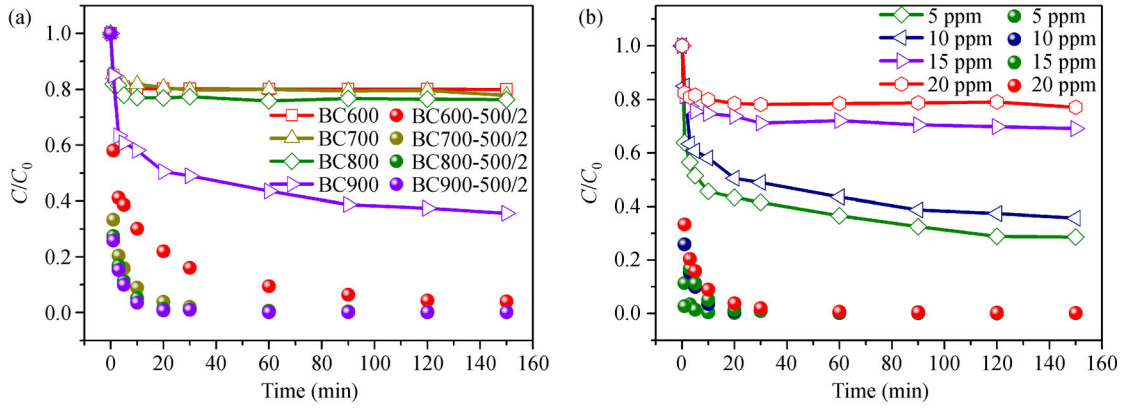

Fig. 7 The removal efficiency of RHB by different BCs (a) (adsorbent dosage = 0.05 g, RHB concentration = 10.0 mg/L, solution volume = 100.0 mL), and the effect of initial concentration on the adsorption of RHB by BC900 and BC900-500/2 (b) (adsorbent dosage = 0.05 g, solution volume = 100.0 mL, lines for BC900 and dots for BC900-500/2).

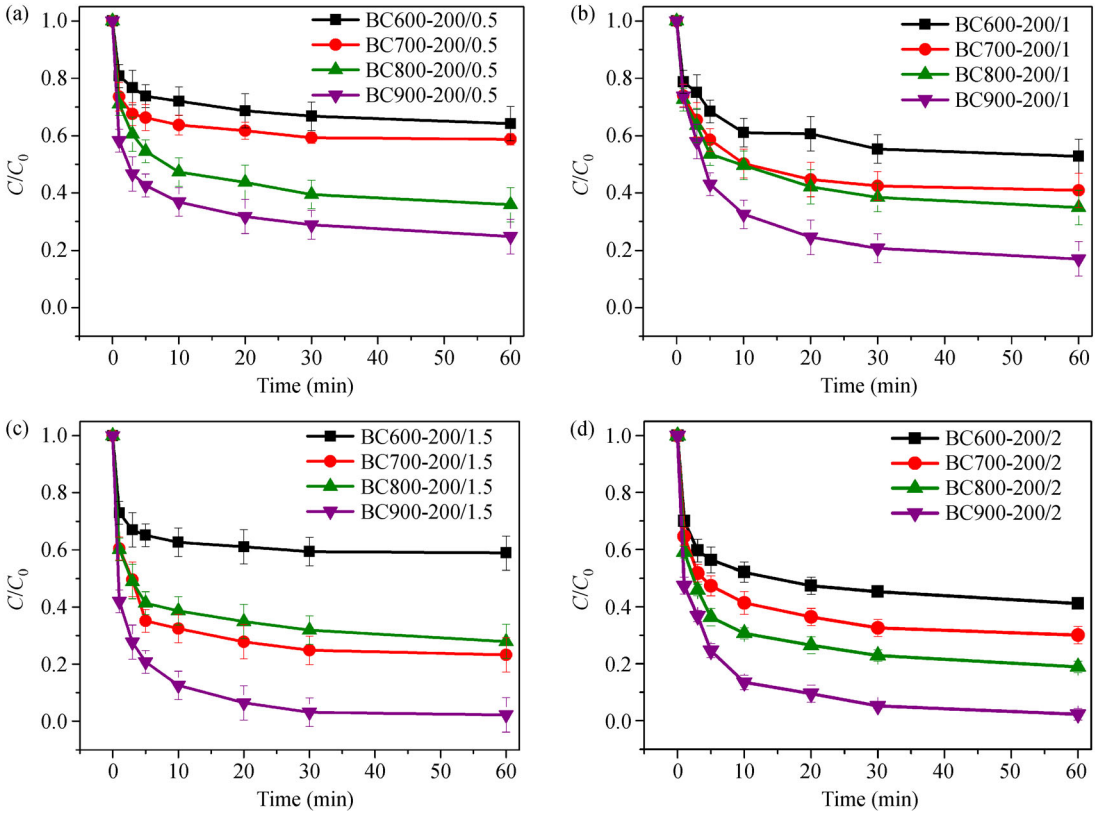

Fig. 8 The effect of ball milling time on the removal efficiency of RHB by BCs. Agitation time = 0.5 h (a), 1 h (b), 1.5 h (c), and 2 h (d) (adsorbent dosage = 0.05 g, RHB concentration = 10.0 mg/L, solution volume = 100.0 mL).

efficiency of pollutants in aqueous solutions by BCs (Qiu et al., 2009; Mohan et al., 2014; Tang et al., 2020b; Xiang et al., 2020), the effect of pH on the adsorption of target pollutants must address. Typically, when the solution pH was less than the point of zero charge pH (pHpzc), extra H^+ or H_3O^+ ions will exist in the solution and may occupy the active sites of BC, resulting in a positively charged adsorbent. In this case, negatively charged pollutants tend to be adsorbed. On the contrary, the negatively charged surface of BCs will trap positively charged pollutants when pH>pHpzc (Qiu et al., 2009; Su et al., 2019). Since MB can react with OH^- to form a purple or dark purple precipitate, and all of the prepared BCs have no adsorption for Cr(VI), RHB was used to investigate the effect of pH on BC adsorption process. The initial solution pH was set to be 2, 4, 6, 8, 10, and 12, and BC900-200/1.5 was selected as adsorbent. For single adsorption, 0.05 g BC900-200/1.5 was added into 100 mL 10 mg/L of RHB solution and the mixture was stirred at 300 r/min for 150 min. As shown in Fig. S5(a), pH has little effect on the removal of RHB by BC900 when pH < 10. By comparison, the removal efficiency decreased to 46.4% at pH = 12. Similarly, the lowest RHB removal efficiency by BC900-200/1.5 obtained at pH = 12, at which the removal efficiency decreased to 89.5% after reaction for 30 min (Fig. S5(b)).

3.6 Adsorption kinetics and isotherm analyses

To disclose the adsorption kinetics which controls the time for equilibrium adsorption at the solid-liquid interface, 0.05 g BC600, BC700, BC800, BC900, and BC900-200/1 (BC900-200/1) were added to remove MB (RHB). As shown in Figs. S6(a) and S6(b), the adsorption proceeded rapidly at the very beginning. After about 5 min, the adsorption reaction slowed down gradually and the adsorption equilibrium reached at about 30 min for MB while 60 min for RHB. The parameters that summarized in Table S1 showed that the R^2 for pseudo-second-order adsorption was all higher than 0.99, which is much higher than that of pseudo-second-order adsorption (Hu et al., 2020; Su et al., 2020a). This is confirmed by the plots in Figs. S6(c) and S6(d). To further investigate the adsorption performance of prepared BCs, the adsorption isotherms were also investigated by Langmuir and Freundlich models. The fitting plots are presented in Figs. S6(e) and S6(f), respectively, and the related parameters are given in Table S2. According to the calculated R^2, the adsorption of MB and RHB by BC600, BC700, BC800, BC900, and BC900-200/1(BC900-200/1) was in line with Langmuir adsorption isotherm, which further proved that the adsorption was chemically dominated (Zhang et al., 2013; Xiao et al., 2019). The adsorption capability of

MB by BC600, BC700, BC800, and BC900 was then calculated to be 1.20, 4.14, 3.06, and 39.36 mg/g, respectively (Fig. 9). By comparison, BC900-500/2 has the highest MB removal capability with 187.36 mg/g. For RHB, the removal amounts by raw BCs are 3.80, 4.58, 5.10, and 12.88 mg/g by BC600, BC700, BC800, and BC900, respectively. After ball milling, the maximum removal capacity of RHB is 36.58 mg/g obtained by BC600-500/2 (Fig. 9).

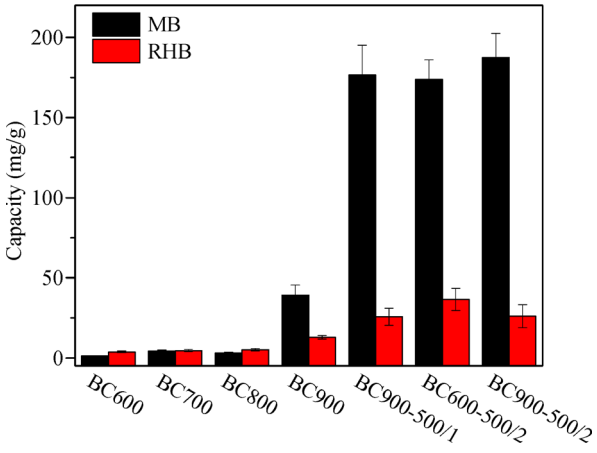

Fig. 9 The adsorption capacity of selected BCs for MB and RHB.

4 Conclusions

This study found that mechanochemical treatment not only improved the adsorption properties of biochar (BC) significantly but also reduced the calcination temperature for the BC preparation. The XRD analysis revealed that graphite was generated during mechanochemical treatment which is speculated to promote the adsorption of organic pollutant. The adsorption tests indicated that the removal amount of MB by BC600, BC700, BC800, and BC900 were only 1.20, 4.14, 3.06, and 39.36 mg/g, respectively. By comparison, the MB removal amount by BC900-500/2 which represents the product of BC900 ball milled at 500 r/min for 2 h reached 187.36 mg/g. For RHB, the removal amounts by raw BCs are 3.80, 4.58, 5.10, and 12.88 mg/g by BC600, BC700, BC800, and BC900, respectively. After mechanochemical treatment, the maximum removal capacity is 36.58 mg/g obtained by BC600-500/2.

Acknowledgements This work was financially supported by the National Natural Science Foundation of China (Grant No. 21777106), the Natural Science Foundation of Guangdong Province, China (No. 2017A030313046) and Basic Research Project of Shenzhen City, China (No. JCYJ20170818093429961).

Credit Author Statement

Peidong Su: Methodology, experimental operation, original draft preparation.

Xiangyu Gao: Manuscript revise, English polish, and result discussion.

Junke Zhang: Adsorption kinetic analysis and sorption isotherms, calculation.

Ridha Djellabi: Language checking.

Bo Yang: Supervision, writing- reviewing and editing.

Qi Wu: Characterization, data analysis.

Zhen Wen: XPS analysis.

Electronic Supplementary Material Supplementary material is available in the online version of this article at https://doi.org/10.1007/s11783-021-1418-2 and is accessible for authorized users.

References

Ajmani A, Patra C, Subbiah S, Narayanasamy S (2020). Packed bed column studies of hexavalent chromium adsorption by zinc chloride activated carbon synthesized from *Phanera vahlii* fruit biomass. Journal of Environmental Chemical Engineering, 8(4): 103825

Ao W, Fu J, Mao X, Kang Q, Ran C, Liu Y, Zhang H, Gao Z, Li J, Liu G, Dai J(2018). Microwave assisted preparation of activated carbon from biomass: A review. Renewable & Sustainable Energy Reviews, 92: 958–979

Bakshi S, Banik C, Rathke S J, Laird D A (2018). Arsenic sorption on zero-valent iron-biochar complexes. Water Research, 137: 153–163

Biswal B P, Chandra S, Kandambeth S, Lukose B, Heine T, Banerjee R (2013). Mechanochemical synthesis of chemically stable isoreticular covalent organic frameworks. Journal of the American Chemical Society, 135(14): 5328–5331

Cheng B H, Zeng R J, Jiang H (2017). Recent developments of post-modification of biochar for electrochemical energy storage. Bioresource Technology, 246: 224–233

Choi J H, Lee C, Cho S, Moon G D, kim B, Chang H, Jang H D (2018). High capacitance and energy density supercapacitor based on biomass-derived activated carbons with reduced graphene oxide binder. Carbon, 132: 16–24

Djellabi R, Zhao X, Bianchi C L, Su P D, Ali J, Yang B (2020). Visible light responsive photoactive polymer supported on carbonaceous biomass for photocatalytic water remediation. Journal of Cleaner Production, (269): 122286

Freundlich H M F (1906). Über die adsorption in lösungen. Zeitschrift für Physikalische Chemie, 57A: 385–470

He L, Tong Z, Wang Z, Chen M, Huang N, Zhang W (2018). Effects of calcination temperature and heating rate on the photocatalytic properties of ZnO prepared by pyrolysis. Journal of Colloid and Interface Science, 509: 448–456

Ho Y S, McKay G (1998). Sorption of dye from aqueous solution by peat. Chemical Engineering Journal, 70(2): 115–124

Hu R, Xiao J, Wang T, Chen G, Chen L, Tian X (2020). Engineering of phosphate-functionalized biochars with highly developed surface area and porosity for efficient and selective extraction of uranium. Chemical Engineering Journal, (379): 122388

Huang Y, Xia S, Lyu J, Tang J (2019). Highly efficient removal of aqueous Hg^{2+} and CH_3Hg^+ by selective modification of biochar with 3-mercaptopropyltrimethoxysilane. Chemical Engineering Journal, 360: 1646–1655

Jonidi Jafari A, Kakavandi B, Jaafarzadeh N, Rezaei Kalantary R, Ahmadi M, Akbar Babaei A (2017). Fenton-like catalytic oxidation

of tetracycline by AC@Fe_3O_4 as a heterogeneous persulfate activator: Adsorption and degradation studies. Journal of Industrial and Engineering Chemistry, 45: 323–333

Julien P A, Užarević K, Katsenis A D, Kimber S A J, Wang T, Farha O K, Zhang Y, Casaban J,Germann L S, Etter M, Dinnebier R E, James S L, Halasz I, Friščić T (2016). In situ monitoring and mechanism of the mechanochemical formation of a microporous MOF-74 framework. Journal of the American Chemical Society, 138(9): 2929–2932

Kim J Y, Oh S, Park Y K (2020). Overview of biochar production from preservative-treated wood with detailed analysis of biochar characteristics, heavy metals behaviors, and their ecotoxicity. Journal of Hazardous Materials, 384: 121356

Kim Y, Oh J I, Vithanage M, Park Y K, Lee J, Kwon E E (2019). Modification of biochar properties using CO_2. Chemical Engineering Journal, 372: 383–389

Kumar M, Xiong X, Wan Z, Sun Y, Tsang D C W, Gupta J, Gao B, Cao X, Tang J, Ok Y S (2020). Ball milling as a mechanochemical technology for fabrication of novel biochar nanomaterials. Bioresource Technology, (312): 123613

Lagergreen S (1898). Zur theorie der sogenannten adsorption gelöster stoffe kungliga svenska vetenskapsakademiens. Handlingar, 24(4): 1–39

Langmuir I (1918). The adsorption of gases on plane surfaces of glass, mica and platinum. Journal of the American Chemical Society, 40(9): 1361–1403

Li H, Mahyoub S A A, Liao W, Xia S, Zhao H, Guo M, Ma P (2017a). Effect of calcination temperature on characteristics and aromatic contaminants adsorption behavior of magnetic BC derived from calcination oil distillation residue. Bioresource Technology, 223: 20–26

Li W, Dang Q, Brown R C, Laird D, Wright M M (2017b). The impacts of biomass properties on calcination yields, economic and environmental performance of the calcination-bioenergy-BC platform to carbon negative energy. Bioresource Technology, 241: 959–968

Li Y, Su P, Li Y, Wen K, Bi G, Cox M (2018). Adsorption-desorption and degradation of insecticides clothianidin and thiamethoxam in agricultural soils. Chemosphere, 207: 708–714

Liu W J, Jiang H, Yu H Q (2015). Development of BC-based functional materials: toward a sustainable platform carbon material. Chemical Reviews, 115(22): 12251–12285

Liu Z, Adewuyi Y G, Shi S, Chen H, Li Y, Liu D, Liu Y (2019). Removal of gaseous Hg^0 using novel seaweed biomass-based activated carbon. Chemical Engineering Journal, 366: 41–49

Lu L, Shan R, Shi Y, Wang S, Yuan H (2019). A novel TiO_2/biochar composite catalysts for photocatalytic degradation of methyl orange. Chemosphere, 222: 391–398

Lu Z, Li Y, Liu T,Wang G, Sun M, Jiang Y, He H, Wang Y, Zou P, Wang X, Zhao Q, Rao H (2020). A dual-template imprinted polymer electrochemical sensor based on AuNPs and nitrogen-doped graphene oxide quantum dots coated on NiS_2/biomass carbon for simultaneous determination of dopamine and chlorpromazine. Chemical Engineering Journal, 389: 124417

Lyu H, Gao B, He F, Zimmerman A R, Ding C, Huang H, Tang J (2018). Effects of ball milling on the physicochemical and sorptive properties of biochar: experimental observations and governing mechanisms. Environmental Pollution, 233: 54–63

Mohan D, Kumar H, Sarswat A, Alexandre-Franco M, Pittman C U Jr (2014). Cadmium and lead remediation using magnetic oak wood and oak bark fast pyrolysis bio-chars. Chemical Engineering Journal, 236: 513–528

Peters J F, Iribarren D, Dufour J (2015). Biomass pyrolysis for biochar or energy applications? A life cycle assessment. Environmental Science & Technology, 49(8): 5195–5202

Qiu Y, Zheng Z, Zhou Z, Sheng G D (2009). Effectiveness and mechanisms of dye adsorption on a straw-based biochar. Bioresource Technology, 100(21): 5348–5351

Rajapaksha A U, Chen S S, Tsang D C W, Zhang M, Vithanage M, Mandal S, Gao B, Bolan N S, Ok Y S (2016). Engineered/designer biochar for contaminant removal/immobilization from soil and water: Potential and implication of biochar modification.. Chemosphere, 148: 276–291

Sizmur T, Fresno T, Akgül G, Frost H, Moreno-Jiménez E (2017). Biochar modification to enhance sorption of inorganics from water. Bioresource Technology, 246: 34–47

Su P, Liu Y, Zhang J, Chen C, Yang B, Zhang C, Zhao X (2020a). Pb-based perovskite solar cells and the underlying pollution behind clean energy: dynamic leaching of toxic substances from discarded perovskite solar cells. Journal of Physical Chemistry Letters, 11(8): 2812–2817

Su P, Zhang J, Tang J, Zhang C (2019). Preparation of nitric acid modified powder activated carbon to remove trace amount of Ni(II) in aqueous solution. Water Science and Technology, 80(1): 86–97

Su P,Zhang J, Xiao K, Zhao S, Djellabi R, Li X, Yang B, Zhao X (2020b). C_3N_4 modified with single layer ZIF67 nanoparticles for efficient photocatalytic degradation of organic pollutants under visible light. Chinese Journal of Catalysis, 41(12): 1894–1905

Sun Y, Gao B, Yao Y, Fang J, Zhang M, Zhou Y, Chen H, Yang L (2014). Effects of feedstock type, production method, and pyrolysis temperature on biochar and hydrochar properties. Chemical Engineering Journal, 240: 574–578

Talukdar K, Jun B M, Yoon Y, Kim Y, Fayyaz A, Park C M (2020). Novel Z-scheme Ag_3PO_4/Fe_3O_4-activated biochar photocatalyst with enhanced visible-light catalytic performance toward degradation of bisphenol A. Journal of Hazardous Materials, 398: 123025

Tang J, Liu Y, Su P, Quan J, Hu Y, Wang W, Zhang C (2020a). Removal of COD, NH_4-N, and perfluorinated compounds from wastewater treatment plant effluent using ZnO-coated activated carbon. Water Science and Technology, 81(11): wst2020308

Tang J, Zhang C, Wang L, Hu Y, Su P, Wang W, He X (2020b). Photo-electrocatalytic degradation of cyclic volatile methyl siloxane by ZnO-coated aluminum anode: Optimal parameters, kinetics, and reaction pathways. Science of the Total Environment, 733: 139246

Teng C, Xie D, Wang J, Yang Z, Ren G, Zhu Y (2017). Ultrahigh conductive graphene paper based on ball-milling exfoliated graphene. Advanced Functional Materials, 27(20): 1700240

Tian Q, Wu W, Yang S, Liu J, Yao W, Ren F, Jiang C (2017). Zinc oxide coating effect for the dye removal and photocatalytic mechanisms of flower-like MoS_2 nanoparticles. Nanoscale Research Letters, 12(1–10): 221

Tran H N, You S J, Hosseini-Bandegharaei A, Chao H P (2017). Mistakes and inconsistencies regarding adsorption of contaminants

from aqueous solutions: A critical review. Water Research, 120: 88–116

Tsuzuki T, McCormick P G (2004). Mechanochemical synthesis of nanoparticles. Journal of Materials Science, 39(16–17): 5143–5146

Xiang W, Wan Y, Zhang X, Tan Z, Xia T, Zheng Y, Gao B. (2020). Adsorption of tetracycline hydrochloride onto ball-milled biochar: Governing factors and mechanisms. Chemosphere, 255: 127057

Xiao J, Hu R, Chen G (2019). Micro-nano-engineered nitrogenous bone biochar developed with a ball-milling technique for high-efficiency removal of aquatic Cd(II), Cu(II) and Pb(II). Journal of Hazardous Materials, 387: 121980

Xu X, Zheng Y, Gao B, Cao X (2019). N-doped biochar synthesized by a facile ball-milling method for enhanced sorption of CO_2 and reactive red. Chemical Engineering Journal, 368: 564–572

Yang H, Hu Y, Zhang X, Qiu G (2004). Mechanochemical synthesis of cobalt oxide nanoparticles. Materials Letters, 58(3–4): 387–389

Yao Y, Lian C, Wu G, Hu Y, Wei F, Yu M, Wang S (2017). Synthesis of "sea urchin"-like carbon nanotubes/porous carbon superstructures derived from waste biomass for treatment of various contaminants. Applied Catalysis B: Environmental, 219: 563–571

Ye S, Yan M, Tan X, Liang J, Zeng G, Wu H, Song B, Zhou C, Yang Y, Wang H (2019). Facile assembled biochar-based nanocomposite with improved graphitization for efficient photocatalytic activity driven by visible light. Applied Catalysis B: Environmental, 250: 78–88

Yu K L, Lau B F, Show P L, Ong H C, Ling T C, Chen W H, Ng E P, Chang J S (2017). Recent developments on algal biochar production and characterization. Bioresource Technology, 246: 2–11

Zhang C, Tan S, Niu X, Su P (2015). Treatment of geothermal water with high fluoride content by electrocoagulation. Desalination and Water Treatment, 54(8): 2223–2227

Zhang C, Wang K, Tan S, Niu X, Su P (2013). Evaluation and remediation of organics, nutrients and heavy metals in landfill leachate: A case study in Beijing. Chemistry and Ecology, 29(8): 668–675

Zhang J, Su P, Li Y, Li L (2020a). Environmental investigation of bio-modification of steel slag through microbially induced carbonate precipitation. Journal of Environmental Sciences-China, 101: 282–292

Zhang J, Zhao H, Li J, Jin H, Yu X, Lei Y, Wang S (2019). In situ encapsulation of iron complex nanoparticles into biomass-derived heteroatom-enriched carbon nanotubes for high-performance super-capacitors. Advanced Energy Materials, 9(4): 1803221

Zhang S, Jiang S F, Huang B C, Shen X C, Chen W J, Zhou T P, Cheng H Y, Cheng B H, Wu C Z, Li W W, Jiang H, Yu H Q (2020b). Sustainable production of value-added carbon nanomaterials from biomass calcination. Nature Sustainability, 2020: 1–8

Zhang Y, Lu L, Zhang S, Lv Z, Yang D, Liu J, Chen Y, Tian X, Jin H, Song W (2018). Biomass chitosan derived cobalt/nitrogen doped carbon nanotubes for the electrocatalytic oxygen reduction reaction. Journal of Materials Chemistry. A, Materials for Energy and Sustainability, 6(14): 5740–5745

Zhang Y, Su P, Weathersby D, Zhang Q, Zheng J, Fan R, Dai Q (2020c). Synthesis of γ-Fe_2O_3-ZnO-biochar nanocomposites for Rhodamine B removal. Applied Surface Science, 501: 144217 : 1-7